Research Article

Mohamad Hamzeh* and Farid Karimipour

An ABC-optimized fuzzy ELECTRE approach for assessing petroleum potential at the petroleum system level

https://doi.org/10.1515/geo-2020-0159
received March 24, 2019; accepted May 24, 2020

Abstract: An inevitable aspect of modern petroleum exploration is the simultaneous consideration of large, complex, and disparate spatial data sets. In this context, the present article proposes the optimized fuzzy ELECTRE (OFE) approach based on combining the artificial bee colony (ABC) optimization algorithm, fuzzy logic, and an outranking method to assess petroleum potential at the petroleum system level in a spatial framework using experts' knowledge and the information available in the discovered petroleum accumulations simultaneously. It uses the characteristics of the essential elements of a petroleum system as key criteria. To demonstrate the approach, a case study was conducted on the Red River petroleum system of the Williston Basin. Having completed the assorted preprocessing steps, eight spatial data sets associated with the criteria were integrated using the OFE to produce a map that makes it possible to delineate the areas with the highest petroleum potential and the lowest risk for further exploratory investigations. The success and prediction rate curves were used to measure the performance of the model. Both success and prediction accuracies lie in the range of 80–90%, indicating an excellent model performance. Considering the five-class petroleum potential, the proposed approach outperforms the spatial models used in the previous studies. In addition, comparing the results of the FE and OFE indicated that the optimization of the weights by the ABC algorithm has improved accuracy by approximately 15%, namely, a relatively higher success rate and lower risk in petroleum exploration.

Keywords: optimization, artificial bee colony algorithm, outranking, fuzzy ELECTRE, petroleum potential, Red River petroleum system, Williston Basin

1 Introduction

In the petroleum industry, the essence of exploration is to convert undiscovered resources to recoverable reserves. Petroleum potential modeling is an important preliminary step in petroleum exploration. There are several approaches for assessing petroleum potential of an area, which can be generally classified as data-driven, knowledge-driven, and hybrid approaches. Data-driven models involve quantitative analysis of spatial relationships between discovered petroleum pools in a region of interest and indirect evidence of petroleum potential. The resulting relationships are used to determine the parameters of the model by which evidence data sets are integrated into a single petroleum potential map. In contrast, knowledge-driven methods rely on the judgments of experts who evaluate the relative importance of input data sets and the model parameters [1].

Despite the fundamental differences, there are the methodological similarities between the mineral prospectivity mapping (MPM) and petroleum potential modeling. It is accordingly worthwhile to first provide a brief summary of the commonly used data- and knowledge-driven methods for predicting mineral prospectivity that can potentially be used to evaluate petroleum resource potential. In recent decades, several data-driven methods have been developed and successfully applied in MPM such as logistic regression [2], weights of evidence (WofE) [3], fuzzy WofE [4], boost WofE [5], support vector machine [6], artificial neural networks [6], Bayesian network classifiers [7], decision tree analysis [8], random forests [9], isolation forest [10], certainty factor [11], extreme learning machines [12], and maximum entropy

* **Corresponding author: Mohamad Hamzeh,** Department of GIS, School of Surveying and Geospatial Engineering, College of Engineering, University of Tehran, Tehran, Tehran 1439957131, Islamic Republic of Iran, e-mail: hamzeh.mohamad@ut.ac.ir, tel: +98-912-286-5483
Farid Karimipour: Department of GIS, University of Tehran, Tehran, Islamic Republic of Iran, e-mail: f.karimipour@ut.ac.ir

[13]. Boolean logic, index overlay [14], wildcat mapping [15], fuzzy logic [16], data envelopment analysis [17], PROMETHEE [1], ELECTRE [18], AHP [19], and TOPSIS [20] are examples of knowledge-driven methods. It is noteworthy that some of the methods like evidential belief functions (EBFs) can be implemented in both frameworks in order to map mineral prospectivity (i.e., data-driven EBF [21] and knowledge-driven EBF [22]).

In the past few years, some researchers have attempted to evaluate petroleum potential using various algorithms. Zargani et al. [23] applied the WofE method successfully to delineate the areas with the highest potential in the Murzuq Basin of Libya for more investigation. Source rock, reservoir rock, migration, and trapping as the main geological factors were combined in a geographic information system (GIS) framework to produce a probability map of hydrocarbon occurrence. The resulting posterior probability map showed that 64% of petroleum accumulations were located in the favorable regions. An approximate fuzzy assessment (AFA) system on the strength of the possibility and fuzzy set theories for petroleum resource evaluation was developed by Tounsi [24]. Although the AFA system considered all essential petroleum system elements and could efficiently deal with imprecise information and incomplete data, it investigated petroleum favorability in a nonspatial framework. Bingham et al. [25] introduced a GIS-based fuzzy multicriteria evaluation model for producing the petroleum potential map. The proposed method was used for frontier exploration areas of northern South America because it works without relying on prior probabilities of the presence of petroleum accumulations. Arab Amiri et al. [26] utilized two data-driven methods, EBF and frequency ratio, to predict the potential distribution of petroleum resources in the Williston Basin. Seven subcriteria of the Red River petroleum system elements were selected as input data sets. The findings indicated that the frequency ratio achieved slightly better performance than the EBF. Ziyong et al. [27] employed a GIS-based fuzzy logic for integrating geological, geophysical, and simulation data in order to investigate the gas potential of the Chu-Sarysu Basin in Kazakhstan. The results of the study were validated by in situ gas testing. A geochemical study was conducted by Lei et al. [28] to delineate the anomaly areas of the Sangnan field in northwestern China for predicting the spatial distribution of petroleum resources. Fifteen petroleum indices from surface soil samples were classified into three classes according to principal component analysis (PCA) and multifractality. Petroleum prospecting areas were then identified by the concentration-area fractal model. The results revealed that the potential areas correspond well with the discovered petroleum sites.

Seraj and Delavar [29] proposed a methodology based on the Dempster–Shafer theory in a GIS framework for assessing risk of play-based petroleum exploration under spatial uncertainty in the Fars domain of Zagros Basin of Iran. In the methodology, the play risk is subdivided into the regional risk elements. The maps of the regional risk elements, referred to as common risk segment (CRS) maps, are produced. The CRS maps of a specific play are combined into a composite common risk segment (CCRS) map, which provides a basis for an estimate of play risk. The results indicated that about 26% of the study area was delineated as the high petroleum potential class by the classified CCRS map and 73.4% of the testing data were correctly predicted by the proposed model. The Dempster–Shafer theory of evidence and fuzzy sets were integrated by Seraj et al. [30] for spatially evaluating geological risk of petroleum exploration. The authors found that 35% of the area of the Fars sedimentary region of Iran has a high risk for petroleum exploration and 75.9% of the testing data confirms this finding. Various spatial approaches such as the fuzzy-belief networks [31], object-based stochastic model [32], multivariate and Bayesian statistical methods [33], geostatistical techniques and Monte-Carlo simulation [34], hybrid fuzzy-probabilistic method [35], Bayesian networks [36], and machine learning [37] have also been used for risk assessment in petroleum exploration.

The optimized fuzzy ELECTRE (OFE) approach is presented in this article for petroleum potential assessment, in which FE provides a robust decision-making framework that has the ability to handle data with uncertainty and the artificial bee colony (ABC) algorithm is used to optimize the model parameters (i.e., weights of the criteria). In order to validate the proposed approach, a case study was conducted in the Red River petroleum system of the Canadian side of the Williston Basin.

No study, to the best of our knowledge, has yet applied outranking or fuzzy outranking methods to petroleum exploration. Experts' knowledge is incorporated as crisp values into the ELECTRE methods, which is not suitable for the petroleum potential modeling, especially in frontier areas, where information about the importance of the criteria is uncertain, incomplete, and ambiguous. Hence, one of the novelties of the current study is the use of the triangular fuzzy (TF) numbers to define weights of the criteria for petroleum resource assessment. Another point to note is that bias is a major challenge in the exploration of oil and gas. Biased expert-elicited values for the model parameters are strongly associated with unsuccessful outcomes and

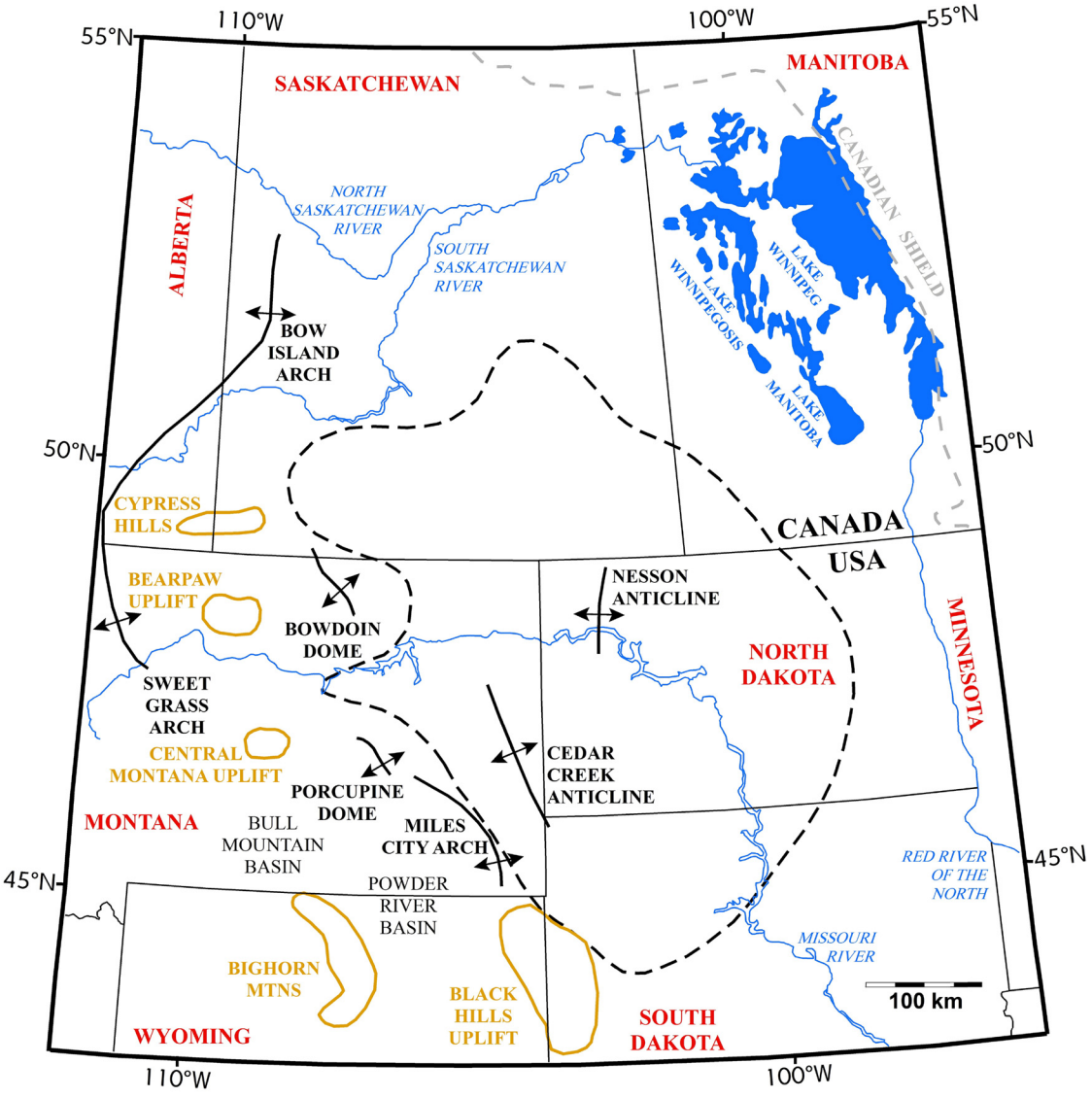

Figure 1: Approximate regional extent of the Williston Basin, represented by the black dashed line (compiled from laird and Folsom [80] and lampen and Rostron [81]).

can lead to a dry hole or an uneconomic reservoir. Accordingly, another important novelty of the presented research work includes the use of the ABC algorithm to optimize the experts-assigned weights of the criteria.

2 Materials and methods

2.1 Geological setting

The Williston Basin is the archetypal intracratonic basin that straddles the United States–Canada border and covers an area of about 3,00,000 square miles [38] across three states in the United States and two provinces in Canada (Figure 1). The concept of petroleum system was first applied in the basin by Williams [39] and Dow [40], who identified three petroleum systems. Further studies reported the presence of seven other petroleum systems, one of which is the Red River, a self-sourced and highly prolific petroleum system that has significant remaining exploration potential [41].

The carbonate succession of the Bighorn Group in Saskatchewan comprises three formations, which are, in ascending order, the Red River, Stony Mountain and Stonewall (Figure 2). The Red River strata is divisible into the Yeoman and Herald Formations on lithological grounds

[42]. Three brining-upward cycles are distinguishable in the strata. The lowest cycle, which is the interval of interest here, consists of the Yeoman Formation and the overlying Lake Alma Member of the Herald Formation. The uppermost third of the Yeoman Formation or Upper Yeoman is strongly mottled, commonly porous, and permeable. These have resulted in relatively good reservoir properties [43,44]. The Upper Yeoman also contains widely distributed, commonly laminated, relatively thin organic-rich interbeds, which are known as kukersites. These interbeds are the major source of hydrocarbons in the Red River petroleum system [45].

Most of the petroleum pools discovered to date in the Red River petroleum system occur mainly in structural traps with stratigraphic enhancement capped by dense evaporitic deposits [46]. The upper evaporitic unit of Lake Alma Member, informally named the Lake Alma anhydrite, forms an extensive and impermeable cap rock for the lowest cycle of the Red River strata [47].

2.2 Criteria identification

According to Magoon and Sánchez [48], "the petroleum system is the naturally occurring hydrocarbon–fluid system in the geosphere." The petroleum system concept provides a basis for evaluating exploration opportunities and is efficiently used to find undiscovered commercial oil and gas accumulations [49]. The source rock, reservoir rock, seal rock, and overburden rock are the essential elements of a petroleum system. The processes affecting a petroleum system include trap formation and the generation–migration–accumulation of petroleum. The elements and processes of a petroleum system must be correctly placed in time and space so that organic matter of a source rock can be converted to oil and gas accumulations [50]. Some characteristics of the essential elements of petroleum system are used here as the criteria to evaluate petroleum potential of the Red River petroleum system. These are explained below.

Effective source rocks satisfy three requirements including quantity, quality, and thermal maturity [51] (Table 1). The amount of petroleum generated and expelled from source rocks is controlled by the total organic carbon (TOC) content, thickness of source rock (D_s), and thermal maturity (T_{max}) [52]. Quality of organic matter in source rocks is measured by the hydrogen index (HI) parameter [53]. In the present study, TOC, D_s, T_{max}, and HI were selected as criteria in order to assess the source rock potential of the Upper Yeoman.

There are two hydrocarbon-volume attributes that determine the volume of hydrocarbon in the prospect: depth to reservoir and the thickness of reservoir rock (D_r) [54]. Unlike D_r, there is no clear relationship between potential of reservoir rock and reservoir depth. In the absence of permeability and porosity data of the Upper Yeoman, D_r was considered as the criterion to evaluate the reservoir rock potential.

The probability of structures that may have trapping potential being present at a given point is indirectly related to curvature (C_r) and roughness (R_r) of reservoir top surface [26,55,56]. Traps in the Red River petroleum system are predominantly structural [46], so C_r and R_r were adopted as the criteria for assessing the potential of traps formed by anticlinal folds and faults, respectively.

A proper cap rock should not only be impervious, but also should form a barrier above and around the reservoir rock. Two other aspects that must be considered in seal evaluation are the extension and thickness of the cap rock (D_c) [57]. The Lake Alma anhydrite extends across almost the entire study area and the sealing ability of this cap rock mainly depends on the thickness parameter [47]. So, D_c was taken into account in analyzing the sealing potential of the Lake Alma anhydrite.

2.3 Data sets and data preparation

The OFE approach can be implemented either pixel or voxel based. This study was carried out in two-dimensional space; all data sets were, therefore, converted to raster grids with spatial resolution of 1,000 m per pixel.

Data sets required for petroleum potential modeling were selected on the basis of the criteria outlined in Section 2.2. Rock-Eval pyrolysis was undertaken on 183 core samples of the source rock to determine TOC, T_{max}, and HI values. These values were then interpolated by the tension spline method (Figure 3a–c). Isopach and structure data were collected from the exploratory and production wells across the Canadian Williston Basin and interpolated by the ordinary kriging method. The resulting isopach grids of the Upper Yeoman (D_s), the reservoir zone of the lowest cycle of the Red River strata (D_r) and the Lake Alma anhydrite (D_c) were used as input data sets for the model (Figure 3d–f).

Surface roughness can be estimated using techniques like roughness index (RI). RI quantifies surface heterogeneity by the following equation [58]:

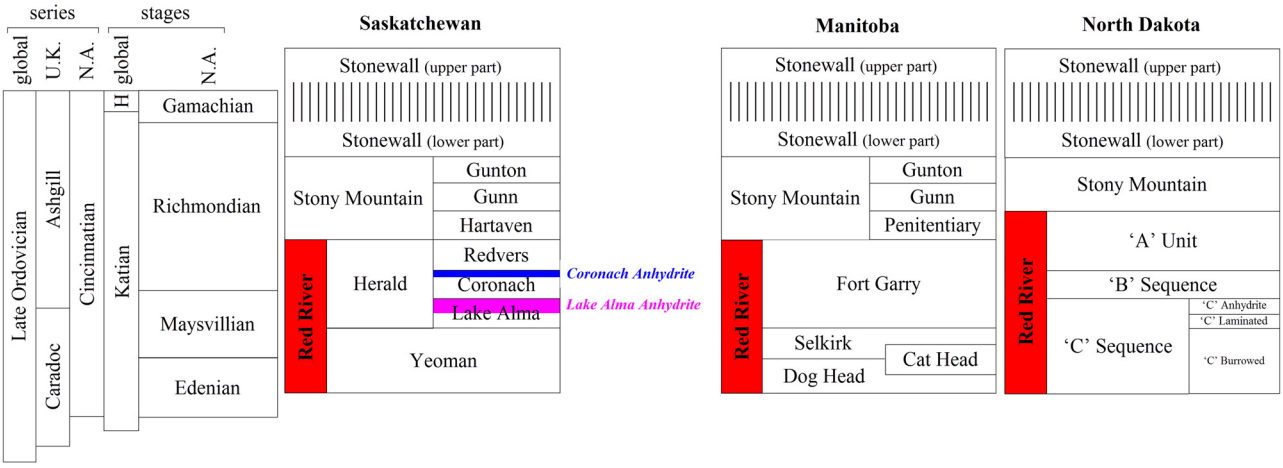

Figure 2: Chronostratigraphy and stratigraphic nomenclature of Upper Ordovician Red River, Stony Mountain, and Stonewall strata in southeastern Saskatchewan and adjacent Manitoba and North Dakota. In global stages, H = Hirnantian (modified from El Taki and Pratt [82]).

$$\mathrm{RI} = Y\left[\left(\sum X_{ij} - X_c\right)^2\right]^{\frac{1}{2}} \quad (1)$$

where X_{ij} is the elevation of each neighbor cell to central cell and X_c is the elevation of central cell. Figure 3g shows R_r data set that is the result of applying RI to structure grid of the reservoir rock.

Curvature is the second derivative of a surface fitted to elevation [59] and measures the convexity or concavity of a surface at a particular pixel. Thus, it can be used for evaluating the trapping potential. C_r data set (Figure 3h) is the second derivative of the structure grid of the reservoir rock.

It should be noted that the sources of all data used in this article are Geoscience Data Repository of Earth Sciences Sector of Natural Resources Canada and the Williston Basin Targeted Geoscience Initiative database [60].

2.4 Methods

2.4.1 The FE approach

The multicriteria analysis (MCA) is useful for problems like petroleum potential analysis in which there are a finite number of spatial elements (pixels or voxels) as alternatives to be assessed on the basis of several, sometimes conflicting, criteria featuring various forms of data and information. Among different methods of MCA, the ELECTRE outranking approach [61] is suitable for finding outranking relations and ranking alternatives [62]. The various ranking formats of the ELECTRE offer several advantages over existing techniques for modeling real-world decision-making problems, the most important of which is the nontotal compensation of multiple criteria aggregation [63]. Another advantage of the ELECTRE methods is that preference and indifference thresholds can easily be considered when modeling partial and imprecise knowledge, which is impossible with other algorithms such as the MAUT, AHP, TOPSIS, MACBETH, SMART, and methods based on fuzzy integrals. Moreover, fuzzy logic [64] is an effective mathematical tool for dealing with uncertainty [35] and is adequate to handle imprecise information and incomplete data in petroleum geology [65]. Consequently, integrating fuzzy logic and FE provides a flexible and effective knowledge-driven framework to model petroleum potential of an area.

The methods of the ELECTRE family are based on m actions ($A_1, A_2, \ldots, A_m$), which will be evaluated according

Table 1: (a) Generative potential (quantity) of immature source rock, (b) kerogen type (quality), and (c) thermal maturity [51]

Potential (quantity)	TOC (wt%)	Kerogen (quality)	HI (mg HC/g TOC)	Maturity	T_{max} (°C)
Poor	<0.5	I	>600	Immature	<435
Fair	0.5–1	II	300–600	Early mature	435–445
Good	1–2	II/III	200–300	Peak mature	445–450
Very good	2–4	III	50–200	Late mature	450–470
Excellent	>4	IV	<50	Postmature	>470
(a)		(b)		(c)	

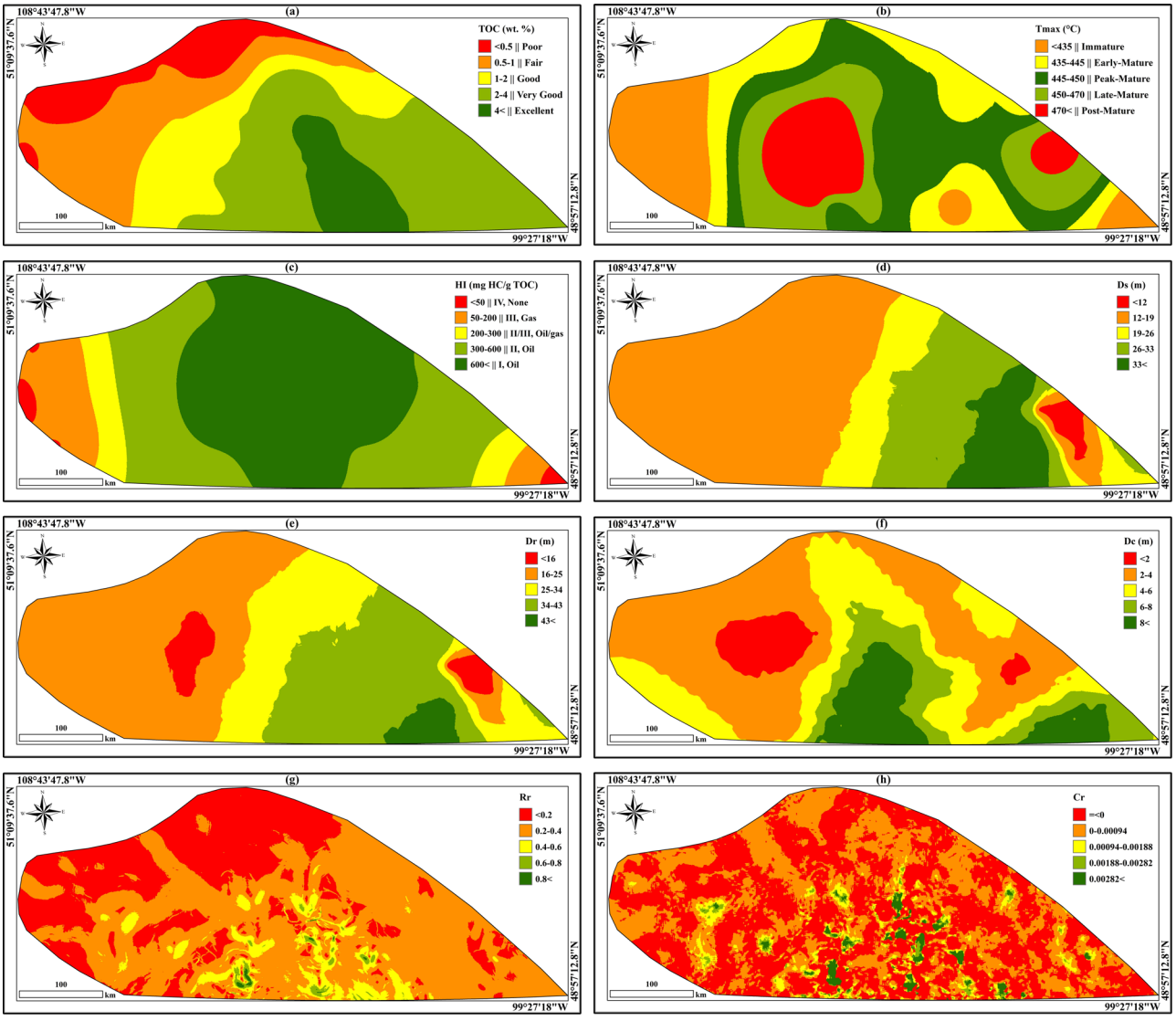

Figure 3: The spatial data layers used in this study: TOC (a), T_{max} (b), HI (c), thickness of the source rock (d), thickness of the reservoir rock (e), thickness of the cap rock (f), RI (g), and curvature (h) maps.

to n criteria ($C_1, C_2, \ldots, C_n$). The FE algorithm can be summarized in the following steps [66]:

Step 1: To begin with, a panel of experts is assembled. Members ($D_1, D_2, \ldots, D_k$) of the group are chosen on the basis of their experience and knowledge in subject areas related to the decision-making problem to be addressed. The members produce a ranking (y_{jk}) of the criteria in increasing order of importance. Next, the aggregate weight of each criterion is defined as TF numbers $\tilde{w} = (a_j, b_j, c_j)$. The aggregate TF weight can be determined as follows:

$$a_j = \min_k\{y_{jk}\}, \quad b_j = \frac{1}{K}\sum_{k=1}^{K} y_{jk}, c_j = \max_k\{y_{jk}\}, \qquad (2)$$

where $k = (1, 2, \ldots, K)$ and $j = (1, 2, \ldots, n)$ are the number of experts and criteria, respectively. The aggregate TF weight for each criterion can then be normalized by the following equation:

$$\tilde{w}_j = (w_{j1}, w_{j2}, w_{j3}), \qquad (3)$$

where

$$w_{j1} = \frac{1/a_j}{\sum_{j=1}^{n} 1/a_j}, \quad w_{j2} = \frac{1/b_j}{\sum_{j=1}^{n} 1/b_j}, \quad w_{j3} = \frac{1/c_j}{\sum_{j=1}^{n} 1/c_j}. \qquad (4)$$

Subsequently, the matrix of normalized aggregate TF weights is formed as $\tilde{W} = (\tilde{w}_1, \tilde{w}_2, \ldots, \tilde{w}_n)$.

Step 2: All the values assigned to the alternatives with respect to each criterion are used to form the decision matrix $X = (x_{ij})_{m\times n}$:

$$X = \begin{bmatrix} x_{11} & x_{12} & \cdots & x_{1n} \\ x_{21} & x_{22} & \cdots & x_{2n} \\ \vdots & \vdots & \ddots & \vdots \\ x_{m1} & x_{m2} & \cdots & x_{mn} \end{bmatrix}. \tag{5}$$

Step 3: The decision matrix is normalized by using the following equations:

$$\begin{cases} r_{ij} = \dfrac{\frac{1}{x_{ij}}}{\sqrt{\sum_{i=1}^{m} \frac{1}{(x_{ij})^2}}} & \text{for minimization objective,} \\ r_{ij} = \dfrac{x_{ij}}{\sqrt{\sum_{i=1}^{m} (x_{ij})^2}} & \text{for maximization objective,} \end{cases} \tag{6}$$

where $i = (1, 2, \ldots, m)$, $j = (1, 2, \ldots, n)$, and r_{ij} represents the normalized preference measure of the ith action in terms of the jth criterion. The normalized decision matrix R can be expressed as:

$$R = \begin{bmatrix} r_{11} & r_{12} & \cdots & r_{1n} \\ r_{21} & r_{22} & \cdots & r_{2n} \\ \vdots & \vdots & \ddots & \vdots \\ r_{m1} & r_{m2} & \cdots & r_{mn} \end{bmatrix}. \tag{7}$$

Step 4: The normalized decision matrix R is then multiplied by TF weights of the evaluation criteria to produce the weighted normalized decision matrix $\tilde{V}$. The matrix $\tilde{V}$ for each criterion is defined using:

$$\begin{aligned} &\tilde{V} = [\tilde{v}_{ij}]_{m\times n} \text{ for } i = (1, 2, \ldots, m) \text{ and} \\ &j = (1, 2, \ldots, n), \text{where } \tilde{v}_{ij} = r_{ij} \times \tilde{w}_j, \end{aligned} \tag{8}$$

and

$$V^1 = \begin{bmatrix} v_{11}^1 & v_{12}^1 & \cdots & v_{1n}^1 \\ v_{21}^1 & v_{22}^1 & \cdots & v_{2n}^1 \\ \vdots & \vdots & \ddots & \vdots \\ v_{m1}^1 & v_{m2}^1 & \cdots & v_{mn}^1 \end{bmatrix},$$

$$V^2 = \begin{bmatrix} v_{11}^2 & v_{12}^2 & \cdots & v_{1n}^2 \\ v_{21}^2 & v_{22}^2 & \cdots & v_{2n}^2 \\ \vdots & \vdots & \ddots & \vdots \\ v_{m1}^2 & v_{m2}^2 & \cdots & v_{mn}^2 \end{bmatrix}, \tag{9}$$

$$V^3 = \begin{bmatrix} v_{11}^3 & v_{12}^3 & \cdots & v_{1n}^3 \\ v_{21}^3 & v_{22}^3 & \cdots & v_{2n}^3 \\ \vdots & \vdots & \ddots & \vdots \\ v_{m1}^3 & v_{m2}^3 & \cdots & v_{mn}^3 \end{bmatrix}.$$

Here $\tilde{v}_{ij}$ denotes normalized positive TF numbers.

Step 5: The concordance and discordance indices are computed for different TF weights of each criterion (i.e., w_{j1}, w_{j2}, w_{j3}). The concordance index C_{pq} measures the degree of concordance with "A_p outranks A_q" and is defined as:

$$C_{pq}^1 = \sum_{j^*} w_{j1}, \quad C_{pq}^2 = \sum_{j^*} w_{j2}, \quad C_{pq}^3 = \sum_{j^*} w_{j3}, \tag{10}$$

where j^* are the attributes contained in $C(p, q)$.

The discordance index D_{pq} represents the discordance degree with the superiority of A_p over A_q and can be formulated as follows:

$$\begin{aligned} D_{pq}^1 &= \frac{\sum_{j^+} |v_{pj^+}^1 - v_{qj^+}^1|}{\sum_j |v_{pj}^1 - v_{qj}^1|}, \\ D_{pq}^2 &= \frac{\sum_{j^+} |v_{pj^+}^2 - v_{qj^+}^2|}{\sum_j |v_{pj}^2 - v_{qj}^2|}, \\ D_{pq}^3 &= \frac{\sum_{j^+} |v_{pj^+}^3 - v_{qj^+}^3|}{\sum_j |v_{pj}^3 - v_{qj}^3|}, \end{aligned} \tag{11}$$

where j^+ are the attributes contained in $D(p, q)$ and v_{ij} is the weighted normalized evaluation of actions i on the criterion j.

Step 6: The final concordance and discordance indices are calculated by the formula (12), which can be considered as the defuzzification process [66].

$$C_{pq}^* = \sqrt[z]{\prod_{z=1}^{Z} C_{pq}^z}, \quad D_{pq}^* = \sqrt[z]{\prod_{z=1}^{Z} D_{pq}^z}, \text{ where } z = 3. \tag{12}$$

The dominance relationship of A_p over A_q becomes stronger with a higher value of C_{pq}^* and a lower value of D_{pq}^*.

Step 7: In order to obtain the ranking of all actions by use of the FE algorithm, some kind of overall outranking needs to be measured. So, following Aouam et al. [67], the overall outranking intensity I was used in this article. $I(A_p)$ measures the overall outranking intensity of A_p over all the other actions. A higher value of $I(A_p)$ reflects a higher attractiveness of A_p [67].

2.4.2 The ABC algorithm

Most knowledge-driven models for petroleum potential assessment such as the FE approach are characterized by complex functional relationships and a large number of parameters that must be determined by experts. In most cases, the model parameters cannot be specified with

precision and the results may suffer from expert subjectivity and bias, hence the need for the parameter optimization. It is a process in which model parameters are tuned for a particular problem. During the last few decades, several tuning techniques have been proposed for optimal tuning of model parameters. Among them, optimization algorithms based on swarm intelligence, known as metaheuristic algorithms, have gained popularity in solving complex and high-dimensional real-world problems. Metaheuristic algorithms generally overcome the drawbacks of conventional or deterministic optimization methods, that is, divergence situations and getting trapped in local optima, because most of them are independent of the initial solutions and are derivative-free [68]. The findings of several studies [69–72] show that the ABC algorithm [73] can outperform other existing techniques such as the genetic algorithms, particle swarm optimization, and differential evolution and is very promising and efficient in solving optimization problems. This is mainly due to the fact that the local and global search of the algorithm are conducted simultaneously in each iteration, so the probability of finding the optimal solutions is considerably increased [74].

The ABC is a simple and robust stochastic algorithm, which simulates the intelligent foraging behavior of honeybee swarms and can be mathematically described as follows.

Suppose N_s denotes the total number of bees, N_u is the size of unemployed bees, N_e denotes the colony size of the employed bees, and $N_s = N_u + N_e$. N_u is usually set to be equal to N_e. If D is the dimension of individual solution vector, then $S = R^D$ and S^{N_e} denote the individual search space and colony space of employed bees, respectively. An employed bee colony can be represented by N_e dimension vector $\overrightarrow{X} = (X_1, X_2, \ldots, X_{N_e})$, where $X_i \in S$, $i \le N_e$. $\overrightarrow{X}(0)$ is the initial employed bee colony and $\overrightarrow{X}(n)$ denotes employed bee colony in the nth iteration. Given the fitness function $f : S \to R^+$, the standard ABC algorithm can be implemented according to the following steps [74]:

Step 1: A set of feasible solutions $(X_1, X_2, \ldots, X_{N_s})$ is initialized randomly and the specific solution X_i can be generated by:

$$X_i^j = X_{\min}^j + \text{rand}(0, 1)(X_{\max}^j - X_{\min}^j) \tag{13}$$

where $j \in \{1, 2, \ldots, D\}$ is the jth dimension of the solution vector. The fitness value of each solution vector is then calculated and the top N_e best solutions are selected to form the initial population of the employed bees $\overrightarrow{X}(0)$.

Step 2: For an employed bee in the nth iteration $X_i(n)$, new solutions are searched in the neighborhood of the current position vector according to the following equation:

$$V_i^j = X_i^j + \varphi_i^j(X_i^j - X_k^j) \tag{14}$$

where $V \in S$, $j \in \{1, 2, \ldots, D\}$, $k \in \{1, 2, \ldots, N_e\}$, $k \neq i$, k, and j are randomly generated, and φ_i^j is a random number in the interval $[-1, 1]$. Generally, this searching process can be denoted as $T_m : S \to S$ because it is a random mapping from individual space to individual space. The probability distribution of the process is related to current position vector $X_i(n)$ but not to the iteration number n and past location vectors.

Step 3: The greedy selection operator $T_s : S^2 \to S$ is applied to choose the better solution between the original vector X_i and searched new vector V_i to proceed into the next generation. Its probability distribution is described as follows:

$$P\{T_s(X_i, V_i) = V_i\} = \begin{cases} 1, & f(V_i) \ge f(X_i), \\ 0, & f(V_i) < f(X_i). \end{cases} \tag{15}$$

The greedy nature of the operator ensures that the population is able to preserve the elite individual, and consequently the evolution will not retreat [75]. It is obvious that the distribution of T_s is not related to the iteration number n.

Step 4: Each unemployed bee picks an employed bee out of the colony according to its fitness value. The probability distribution of the selection operator $T_{s1} : S^{N_e} \to S$ can be described by the following equation:

$$P\{T_{s1}(\overrightarrow{X}) = X_i\} = \frac{f(X_i)}{\sum_{m=1}^{N_e} f(X_m)} \tag{16}$$

Step 5: The neighborhood of the selected employed bee is explored by the unemployed bee to find new solutions. The updated best fitness value is detected as f_{best}, and parameters of the best solution can be expressed as $(x_1, x_2, \ldots, x_D)$.

Step 6: If the search of the neighborhood of an employed bee Bas ends at a specified stopping time $\tau_{\lim}$ without finding better solutions, the location vector will be randomly reinitialized according to the following equation.

$$X_i(n+1) = \begin{cases} X_{\min} + \text{rand}(0, 1)(X_{\max} - X_{\min}), & \text{Bas}_i \ge \tau_{\lim}, \\ X_i(n), & \text{Bas}_i < \tau_{\lim}. \end{cases} \tag{17}$$

Step 7: If the current iteration number is greater than the predefined threshold (i.e., $T > T_{\max}$), output the optimal fitness value f_{best} and associated parameters $(x_1, x_2, \ldots, x_D)$, otherwise go to Step 2.

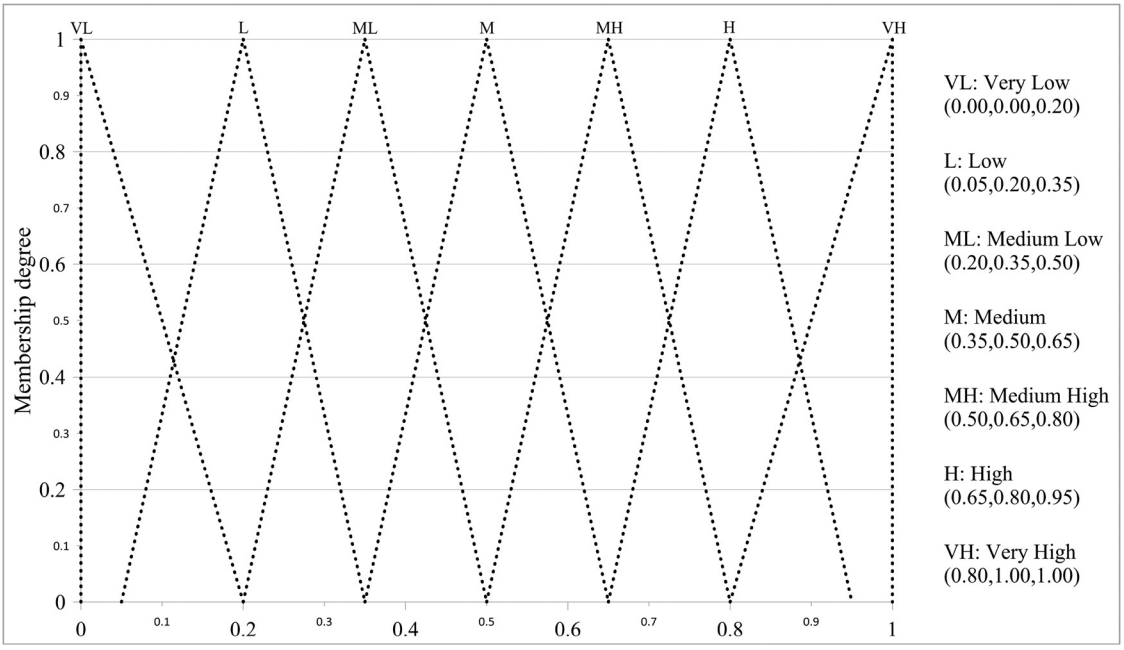

Figure 4: The linguistic variables and their representation as TF numbers.

Step 8: It is the most important aspect of the ABC algorithm that makes it distinctly different from other metaheuristic optimization methods because it diversifies the population to avoid getting trapped in local optima. Obviously, this step can significantly increase the probability of finding an optimal solution [74].

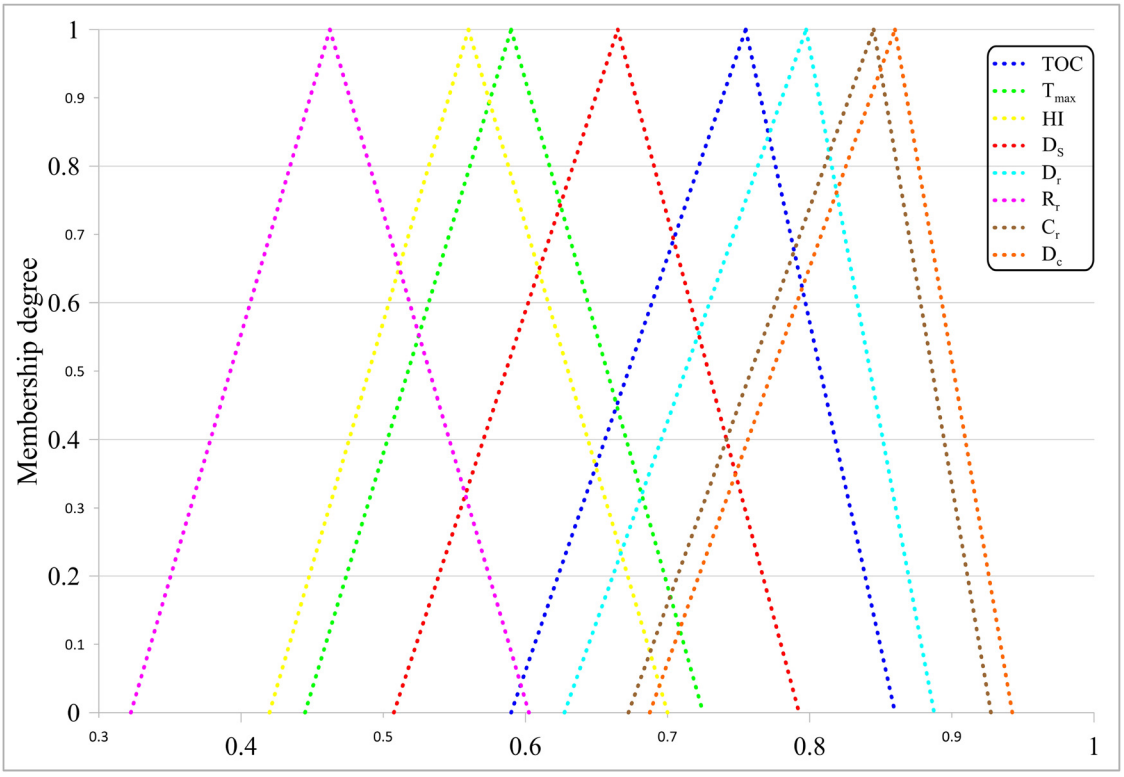

Figure 5: The graphical representation of aggregate weights of the criteria.

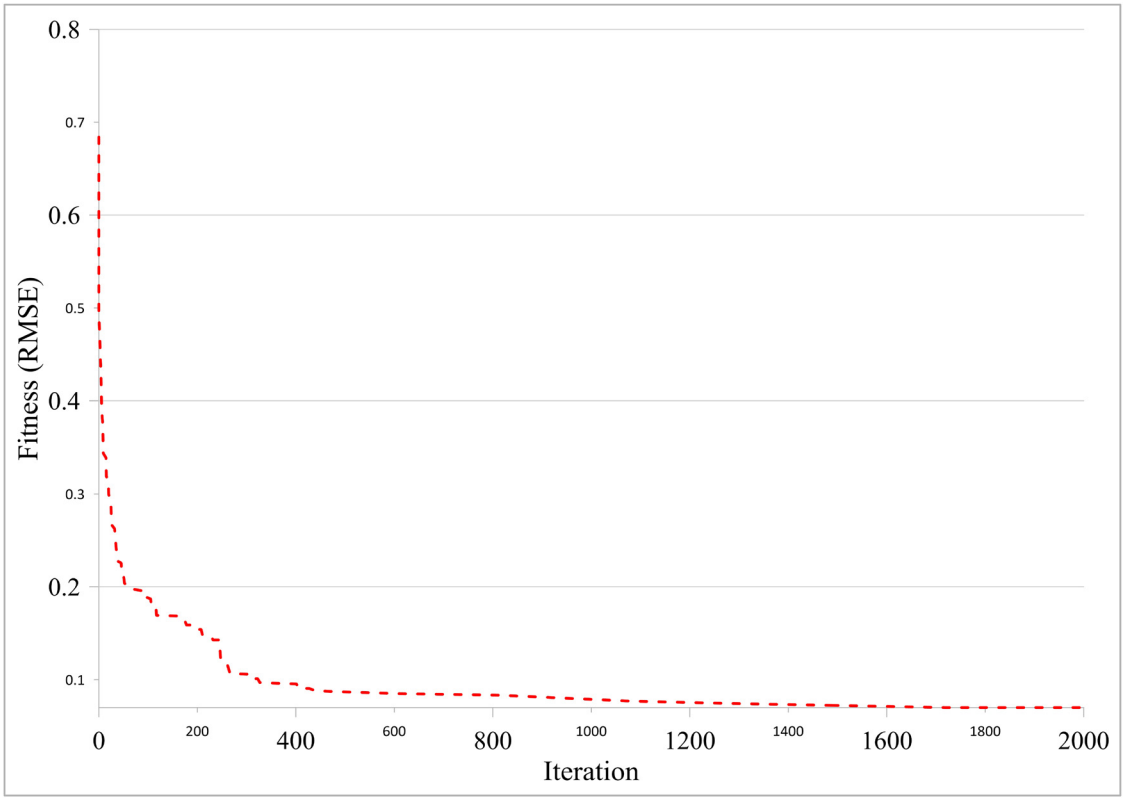

Figure 6: The fitness convergence of the ABC algorithm.

3 Application and results

3.1 Implementation of the FE approach

Cell values of the eight raster data sets described in Section 2.3 were extracted into a table with eight fields as criteria and records as alternatives. In order to apply the FE approach, a vector containing TF weights must first be defined. To this end, the exploration experts participating in the present study were asked to assign one of the seven linguistic variables shown in Figure 4 to each criterion. This linguistic variable represents the relative contribution of each criterion to the overall petroleum potential as a TF number. The variables assigned by different experts were combined by fuzzy simple additive weighting [76] to obtain a TF weight for each criterion. The aggregate weights of the criteria are illustrated as TF numbers in Figure 5.

The values of the overall outranking intensity index (I) were calculated by means of equations (2)–(12) and methodology proposed by Aouam et al. [67]. Finally, I_{norm} values were generated by normalizing the FE outputs to the interval $[0, 1]$.

3.2 Optimization of TF weights of the criteria by the ABC algorithm

The accuracy in determining the parameters of knowledge-driven models such as FE by the experts is dependent on many factors including complexity of the research object, expert qualification, the scale of evaluation, the number of criteria to be evaluated, etc. For example, complicated models with a large number of criteria may suffer from expert-elicited values of parameters. For experts who contributed to this study, there was noticeably higher ambiguity in determining weights of the criteria than others. Therefore, the experts-assigned weights were optimized using the ABC algorithm to obtain more accurate results.

Prior to optimization process, the vector layer of all thirteen discovered oil pools of the Red River petroleum system was rasterized to a 1,000 m cell size grid. Pixels of the grid were randomly subdivided into training and testing subsets with a 70%–30% ratio. The training subset was used in the optimization process to estimate the model parameters, and the testing subset was used to evaluate the predictive power of the model.

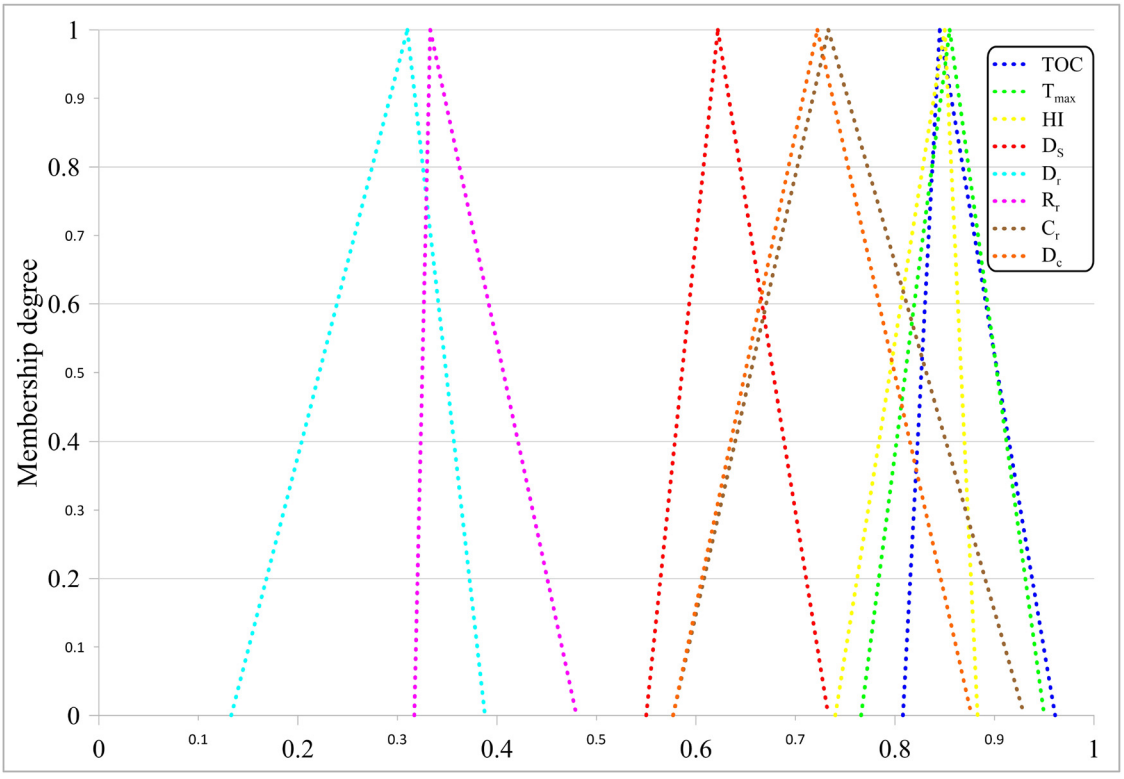

Figure 7: The optimized TF weights of the criteria.

In order to determine the optimal values of the weights, the optimization objective function needs to be first defined. The objective function, in fact, is an indicator of agreement between actual and calculated values of the variable of interest. In this article, root mean square error (RMSE) was selected as the objective function to be minimized in the optimization process. The formula to calculate RMSE is:

$$\mathrm{RMSE} = \sqrt{\frac{1}{n}\sum_{i=1}^{n}(I_{\mathrm{norm,cal},i} - I_{\mathrm{norm,act},i})^2} \tag{18}$$

where $I_{\mathrm{norm,cal},i}$ is the model-calculated value for the ith alternative (pixel) of training subset, $I_{\mathrm{norm,act},i}$ is the actual value of I_{norm} for the same alternative, and $i = 1, 2,\ldots,n$, where n is the total number of pairs of the calculated and actual values. Ideally, $I_{\mathrm{norm,act}}$ should

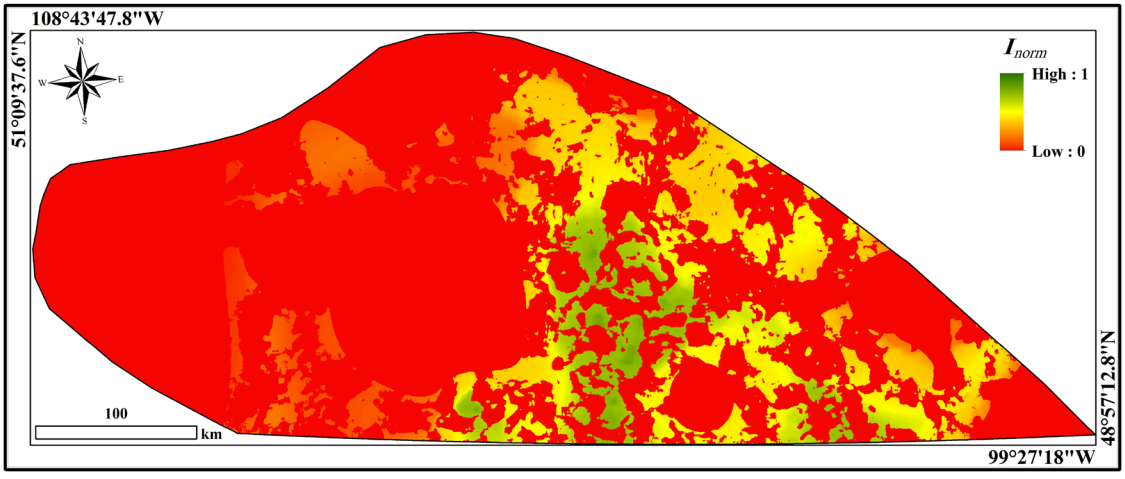

Figure 8: The petroleum potential map of the Red River petroleum system produced by the OFE approach.

Table 2: Attributes of petroleum potential classes

Class	Petroleum potential	I_{norm}	Area (%)	Area of discovered pools located in class (%)
N	No potential	0.0–0.2	76.01	8.03
VL	Very low	0.2–0.4	4.08	0
L	Low	0.4–0.6	13.69	8.26
M	Moderate	0.6–0.8	5.15	4.96
H	High	0.8–1.0	1.07	78.75

be equal to one, the highest value an alternative can have.

A TF number can be represented by $\tilde{\alpha} = (m;\alpha;\beta)$, where m, α, and β are the center, left spread, and right spread, respectively. Thus, twenty-four (8×3) parameters should be optimized when determining the optimal values of the TF weights: In the continuous search space, five constraints were also taken into account:

$$\text{constraints} = \begin{cases} 0 \le m \le 1, \\ 0 \le m - \alpha \le 1, \\ 0 \le m + \beta \le 1, \\ m - \alpha < m + \beta, \\ m - \alpha < m < m + \beta. \end{cases} \tag{19}$$

The control parameters of the ABC algorithm including the colony size and maximum evaluation number were set to 50 and 2,000, respectively. The objective function values obtained by the ABC algorithm versus the number of iterations are depicted in Figure 6. Figure 7 also shows the optimized TF weights of the criteria.

3.3 Implementation of the OFE approach

The optimized TF numbers were used as weights of the criteria in FE to construct the OFE approach. The I_{norm} values computed with OFE were converted to a raster data set at 1,000 m resolution. The resulting potential map of the Red River petroleum system that was

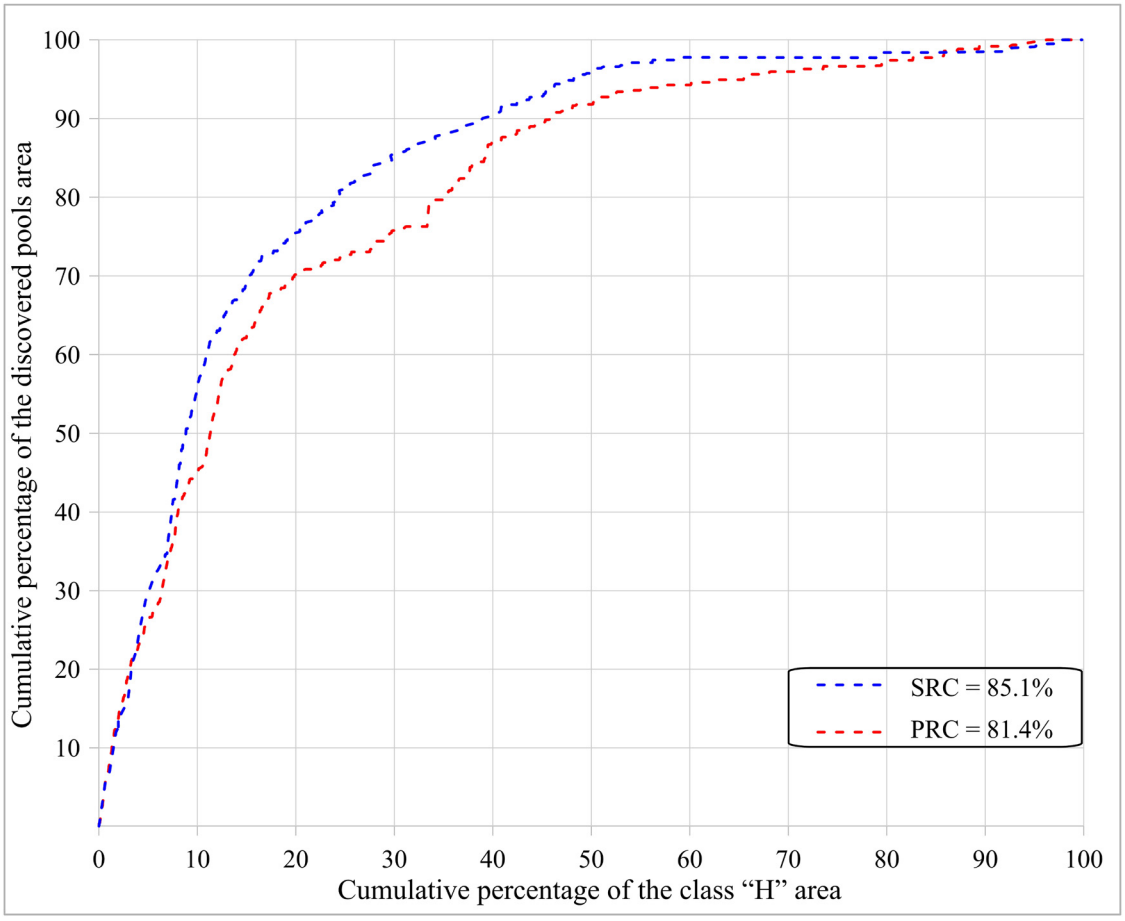

Figure 9: SRC and PRC for OFE.

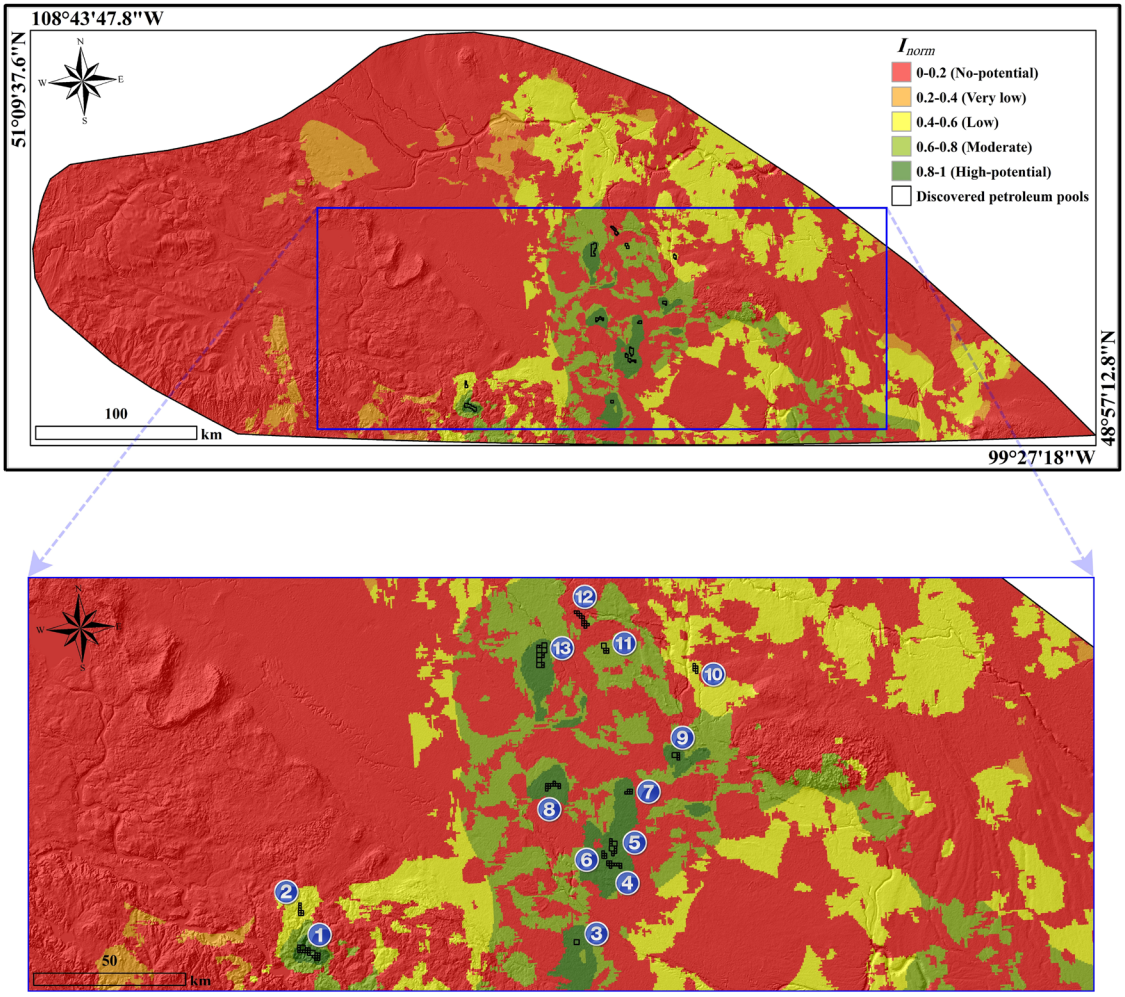

Figure 10: Vector layer of the discovered petroleum pools overlaid on the map obtained from the OFE approach. Blue circled numbers on the map refer to pool numbers given in Table 3.

smoothed by a 3 × 3 pixel median filter is illustrated in Figure 8. The higher the pixel (alternative) value, the greater the petroleum potential is present.

3.4 Validation of the proposed approach

In order to validate the approach, I_{norm} values resulting from OFE were first reclassified into five classes ranging from no to high potential (Table 2). The class "H" with I_{norm} values ranging from 0.8 to 1 along with training and testing subsets were used toward this end. There are several ways to evaluate the performance of a petroleum potential model, among which the success rate curve (SRC) and prediction rate curve (PRC) are the most commonly used methods. Assuming that the model is correct, SRC estimates the goodness of fit, while PRC evaluates the predictive power of the model [77], both of which were used here to measure the performance of OFE. SRC was obtained by plotting the cumulative percentage of the class "H" area on the *x*-axis and the cumulative percentage of the discovered pools area in the training subset on the *y*-axis. PRC was calculated in a similar way as SRC but using the testing subset. The area under the curve (AUC) was then summed to get an efficiency score. SRC and PRC are plotted in Figure 9. As shown in the figure, AUC for SRC (upper dashed line) is 0.851, which corresponds to 85.1% of success accuracy. The area under PRC (lower dashed line) is 0.814 implying a prediction accuracy of 81.4% for the petroleum potential model.

4 Discussion

Exploration in the petroleum industry is an expensive, risky, and increasingly difficult, but necessary, operation.

Table 3: Attributes of petroleum pools used in the verification process

No. (circled numbers in Figure 10)	Pool name	Area (km^2)	I_{norm} range	I_{norm} mean	Class
1	Minton	16.254	0.833–0.961	0.878	H (100%)
2	South Hardy	4.547	0.502–0.588	0.569	L (100%)
3	Bromhead	2.601	0.898–0.951	0.927	H (100%)
4	South Midale	6.476	0.891–0.979	0.956	H (100%)
5	Midale	10.286	0.937–0.981	0.961	H (100%)
6	West Midale	3.243	0.885–0.908	0.900	H (100%)
7	Froude	3.244	0.873–0.911	0.899	H (100%)
8	Mansur	7.136	0.890–0.968	0.922	H (100%)
9	Hartaven	4.513	0.907–0.921	0.913	H (100%)
10	Bemersyde	3.879	0.518–0.559	0.544	L (100%)
11	Montmartre	5.190	0.753–0.779	0.766	M (100%)
12	Chapleau Lake	8.383	0.027–0.756	0.051	N (97.5%) and M (2.5%)
13	Tyvan	19.456	0.871–0.965	0.916	H (100%)

Therefore, to reduce both the costs and risks associated with exploration, a robust and efficient petroleum potential model is expected to lead to high-accuracy results. Both success and prediction accuracies of OFE lie in the range of 80–90%, indicating an excellent model performance [78,79]. In addition, overlaying the vector layer of the discovered oil pools on the reclassified map (Figure 10) showed 78.75% of the area of the pools has been located in the class "H." Comparing the results of the FE and OFE approaches indicated that the optimization of the weights by the ABC algorithm has improved accuracy by approximately 15%, namely, a relatively higher success rate and lower risk in petroleum exploration.

It is difficult to compare the results of the current study to those carried out previously since geological conditions, type and number of criteria, number of potential classes, the area ratio of the potential classes, and techniques of validation vary greatly in the literature. Nevertheless, considering the five-class petroleum potential, the OFE approach with the success and prediction rates of 85.1% and 81.4%, respectively, outperforms the spatial models used in previous similar studies that have been cited here.

Another point to be taken into account is the ratio of the class "H" area to the total area under study, which has an inverse relationship with the screening ability of the petroleum potential model. A smaller ratio is indicative of a smaller area, which needs to be investigated in more detail to find the undiscovered petroleum accumulations. Generally, the lower the area, the lower the cost of exploration. As shown in Table 2, the ratio value for the class "H" of the OFE approach is about 0.01, which is significantly lower compared to those obtained in earlier studies.

The resultant map in Figure 10 clearly shows that the central part of the Canadian side of the Williston Basin has the highest petroleum potential. As summarized in Table 3, the entire area of nine discovered pools including the Bromhead, South Midale, Midale, West Midale, Froude, Mansur, Hartaven, Tyvan, and Minton are located in the class "H." The Montmartre has the moderate petroleum potential. The South Hardy and Bemersyde lie in the class "L," and the Chapleau Lake is mostly located in no-potential class. The box plots of the key criteria for the discovered pools (Figure 11) clearly show that the Montmartre, Bemersyde, and Chapleau Lake are likely to have different trapping mechanisms and the South Hardy probably has a source rock other than the kukersites of the Upper Yeoman.

5 Conclusions

The present study proposes a new approach based on combining an outranking method, fuzzy logic, and the ABC optimization algorithm for assessing petroleum potential using the characteristics of petroleum system elements in a spatial framework. The proposed OFE approach brings together flexibility and simplicity for DMs to solve petroleum exploration problem using experts' knowledge and the information associated with the discovered petroleum pools simultaneously. Having completed the necessary preprocessing steps, eight data sets related to the selected key criteria were integrated by the OFE approach to create a map that makes it possible to identify the areas with the highest petroleum resource potential and the lowest exploration risk.

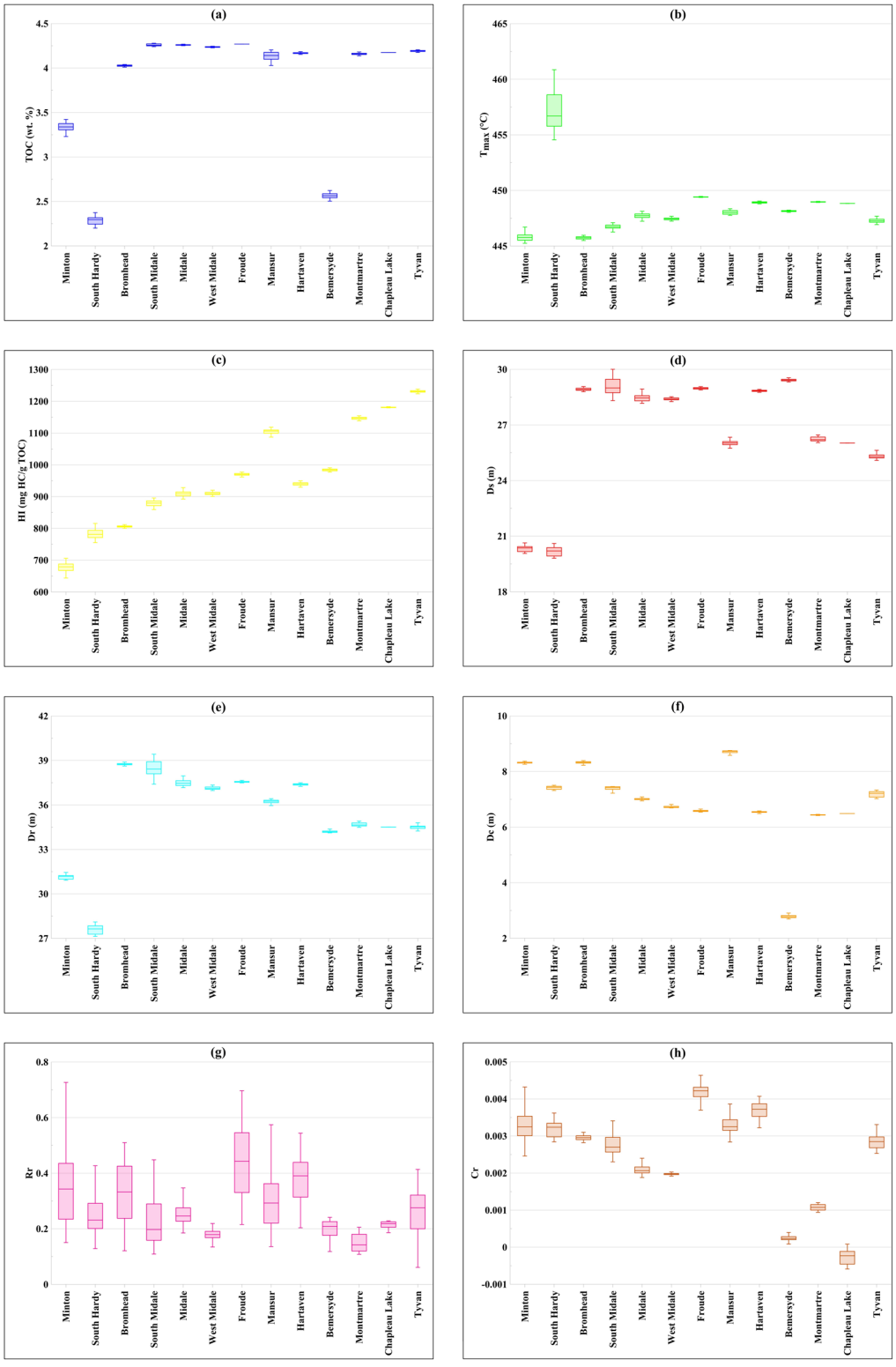

Figure 11: Box plots of the key criteria for the discovered pools of the Red River petroleum system: TOC (a), T_{max} (b), HI (c), thickness of the source rock (d), thickness of the reservoir rock (e), thickness of the cap rock (f), RI (g), and curvature (h).

All discovered oil accumulations in the Canadian part of the Red River petroleum system were used in the verification process. The verification results showed that the proposed method can deal effectively with incomplete data and imprecise information and can be efficiently applied in petroleum exploration. Furthermore, a comparison between

the results of using the experts-assigned weights and optimized weights indicated that the ABC algorithm has the ability to successfully estimate the model parameters and lead to a considerable gain in the accuracy of the model.

In future studies, the model can be improved using other types of preference functions and by optimizing all the model parameters. Moreover, utilizing additional data sets such as permeability and porosity of reservoir rock, which was inaccessible in the present study, is expected to increase the accuracy of the model. The optimal placement of exploratory and production wells requires a robust ranking algorithm with fine-tuned parameters that has the capability to handle data with high uncertainty. Therefore, it is recommended that further studies be undertaken to determine optimal well locations using the proposed approach.

Acknowledgments: The authors would like to thank Mr. Kirk Osadetz from CMC Research Institutes, Inc., and Ms. Jessica Flynn from Saskatchewan Geological Survey for much helpful advice on the geological setting of the Red River petroleum system. Thanks also to the anonymous reviewers and the editor for the helpful comments on an earlier version of this manuscript.

References

[1] Abedi M, Torabi SA, Norouzi GH, Hamzeh M, Elyasi GR. Promethee II: a knowledge-driven method for copper exploration. Comput Geosci. 2012;46:255–63. doi: 10.1016/j.cageo.2011.12.012.

[2] Mejía-Herrera P, Royer JJ, Caumon G, Cheilletz A. Curvature attribute from surface-restoration as predictor variable in kupferschiefer copper potentials. Nat Resour Res. 2015;24:275–90. doi: 10.1007/s11053-014-9247-7.

[3] Qin Y, Liu L. Quantitative 3D association of geological factors and geophysical fields with mineralization and its significance for ore prediction: an example from Anqing Orefield, China. Minerals. 2018;8:300. doi: 10.3390/min8070300.

[4] Zhang Z, Zuo R, Xiong Y. A comparative study of fuzzy weights of evidence and random forests for mapping mineral prospectivity for skarn-type FE deposits in the southwestern Fujian metallogenic belt, China. Sci China Earth Sci. 2016;59:556–72. doi: 10.1007/s11430-015-5178-3.

[5] Cheng Q. Boost wofe: a new sequential weights of evidence model reducing the effect of conditional dependency. Math Geosci. 2015;47:591–621. doi: 10.1007/s11004-014-9578-2.

[6] Sun T, Chen F, Zhong L, Liu W, Wang Y. GIS-based mineral prospectivity mapping using machine learning methods: a case study from Tongling Ore District, Eastern China. Ore Geol Rev. 2019;109:26–49. doi: 10.1016/j.oregeorev.2019.04.003.

[7] Ibrahim AM, Bennett B, Isiaka F. The optimisation of Bayesian classifier in predictive spatial modelling for secondary mineral deposits. Procedia Comput Sci. 2015;61:478–85. doi: 10.1016/j.procs.2015.09.194

[8] Reddy RKT, Bonham-Carter GF. A decision-tree approach to mineral potential mapping in snow lake area, Manitoba. Can J Remote Sens. 1991;17:191–200. doi: 10.1080/07038992.1991.10855292.

[9] Carranza EJM, Laborte AG. Data-driven predictive mapping of gold prospectivity, Baguio District, Philippines: application of random forests algorithm. Ore Geol Rev. 2015;71:777–87. doi: 10.1016/j.oregeorev.2014.08.010.

[10] Chen Y, Wu W. Isolation forest as an alternative data-driven mineral prospectivity mapping method with a higher data-processing efficiency. Nat Resour Res. 2019;28:31–46. doi: 10.1007/s11053-018-9375-6.

[11] Chen YL. Indicator pattern combination for mineral resource potential mapping with the general c–f model. Math Geol. 2003;35:301–21. doi: 10.1023/A:1023870231452.

[12] Chen YL, Wu W. Mapping mineral prospectivity using an extreme learning machine regression. Ore Geol Rev. 2017;80:200–13. doi: 10.1016/j.oregeorev.2016.06.033.

[13] Liu Y, Zhou K, Zhang N, Wang J. Maximum entropy modeling for orogenic gold prospectivity mapping in the Tangbale-Hatu belt, Western Junggar, China. Ore Geol Rev. 2018;100:133–47. doi: 10.1016/j.oregeorev.2017.04.029.

[14] Rezaei S, Lotfi M, Afzal P, Jafari MR, Meigoony MS, Khalajmasoumi M. Investigation of copper and gold prospects using index overlay integration method and multifractal modeling in saveh 1:1,00,000 sheet, Central Iran. Gospod Surowcami Min. 2015;31:51–74. doi: 10.1515/gospo-2015-0038.

[15] Carranza EJM. Improved wildcat modelling of mineral prospectivity. Resour Geol. 2010;60:129–49. doi: 10.1111/j.1751-3928.2010.00121.x.

[16] Elliott BA, Verma R, Kyle JR. Prospectivity modeling for cambrian–ordovician hydraulic fracturing sand resources around the llano uplift, Central Texas. Nat Resour Res. 2016;25:389–415. doi: 10.1007/s11053-016-9291-6.

[17] Hosseini SA, Abedi M. Data envelopment analysis: a knowledge-driven method for mineral prospectivity mapping. Comput Geosci. 2015;82:111–9. doi: 10.1016/j.cageo.2015.06.006.

[18] Abedi M, Torabi SA, Norouzi GH, Hamzeh M. Electre III: a knowledge-driven method for integration of geophysical data with geological and geochemical data in mineral prospectivity mapping. J Appl Geophy. 2012b;87:9–18. doi: 10.1016/j.jappgeo.2012.08.003.

[19] Asadi HH, Sansoleimani A, Fatehi M, Carranza EJM. An AHP – topsis predictive model for district-scale mapping of porphyry Cu–Au potential: a case study from salafchegan area (Central Iran). Nat Resour Res. 2016;25:417–29. doi: 10.1007/s11053-016-9290-7.

[20] Abedi M, Norouzi GH. A general framework of topsis method for integration of airborne geophysics, satellite imagery, geochemical and geological data. Int J Appl Earth Obs Geoinf. 2016;46:31–44. doi: 10.1016/j.jag.2015.11.016.

[21] Carranza EJM. Data-driven evidential belief modeling of mineral potential using few prospects and evidence with missing values. Nat Resour Res. 2015;24:291–304. doi: 10.1007/s11053-014-9250-z.

[22] Tangestani MH, Moore F. The use of Dempster–Shafer model and GIS in integration of geoscientific data for porphyry copper potential mapping, north of Shahr-e-Babak, Iran. Int J Appl Earth Obs Geoinf. 2002;4:65–74. doi: 10.1016/S0303-2434(02)00008-9.
[23] Zargani SS, Vaughan RA, Missallati AA. Spatial integration of geological datasets for predictive hydrocarbon studies in Murzuq Basin, SW Libya. In Geoscience and Remote Sensing Symposium, Toulouse, France. Toulouse, France: IEEE; 2003. p. 991–3. doi: 10.1109/IGARSS.2003.1293988.
[24] Tounsi M. An approximate reasoning based technique for oil assessment. Expert Syst Appl. 2005;29:485–91. doi: 10.1016/j.eswa.2005.05.001.
[25] Bingham L, Zurita-Milla R, Escalona A. Geographic information system-based fuzzy-logic analysis for petroleum exploration with a case study of Northern South America. Am Assoc Pet Geol Bull. 2012;96:2121–42. doi: 10.1306/04251212009.
[26] Arab Amiri M, Karimi M, Alimohammadi Sarab A. Hydrocarbon resources potential mapping using evidential belief functions and frequency ratio approaches, Southeastern Saskatchewan, Canada. Can J Earth Sci. 2015a;52:182–95. doi: 10.1139/cjes-2013-0193.
[27] Ziyong Z, Hangyu Y, Xiaodan G. Fuzzy fusion of geological and geophysical data for mapping hydrocarbon potential based on GIS. Pet Geosci. 2017;24:131–41. doi: 10.1144/petgeo2016-100.
[28] Lei L, Xie S, Chen Z, Carranza EJM, Bao Z, Cheng Q, et al. Distribution patterns of petroleum indices based on multi-fractal and spatial PCA. J Petrol Sci Eng. 2018;171:714–23. doi: 10.1016/j.petrol.2018.07.081.
[29] Seraj S, Delavar MR. An extended GIS-based Dempster–Shafer theory for play-based hydrocarbon exploration risk analysis under spatial uncertainty conditions, case study: Zagros Sedimentary Basin, Iran. Georisk. 2018;13:131–44. doi: 10.1080/17499518.2018.1532522.
[30] Seraj S, Delavar MR, Rezaee R. A hybrid GIS-assisted framework to integrate Dempster–Shafer theory of evidence and fuzzy sets in risk analysis: an application in hydrocarbon exploration. Geocarto Int. 2019:1–19. doi: 10.1080/10106049.2019.1622602.
[31] Xie H, Guo Q, Li F, Li J, Wu N, Hu S, et al. Prediction of petroleum exploration risk and subterranean spatial distribution of hydrocarbon accumulations. Pept Sci. 2011;8:17–23. doi: 10.1007/s12182-011-0110-8.
[32] Chen Z, Hu S, Jin Z, Pang X, Jiang Z, Osadetz GK. Exploration risk evaluation using object-based modeling, an example from the tertiary fractured play, western qaidam basin of china. Pept Sci. 2008;5:195–202. doi: 10.1007/s12182-008-0031-3.
[33] Chen Z, Osadetz KG. Geological risk mapping and prospect evaluation using multivariate and Bayesian statistical methods, western Sverdrup basin of Canada. Am Assoc Pet Geol Bull. 2006;90:859–72. doi: 10.1306/01160605050.
[34] Ruffo P, Bazzana L, Consonni A, Corradi A, Saltelli A, Tarantola S. Hydrocarbon exploration risk evaluation through uncertainty and sensitivity analyses techniques. Reliab Eng Syst Safety. 2006;91:1155–62. doi: 10.1016/j.ress.2005.11.056.
[35] Roisenberg M, Schoeninger C, da Silva RR. A hybrid fuzzy-probabilistic system for risk analysis in petroleum exploration prospects. Expert Syst Appl. 2009;36:6282–94. doi: 10.1016/j.eswa.2008.07.060.
[36] Martinelli G. Petroleum exploration with Bayesian networks: from prospect risk assessment to optimal exploration. Oslo: Norwegian University of Science and Technology; 2012.
[37] Dell'Aversana P, Ciurlo B, Colombo S. Integrated geophysics and machine learning for risk mitigation in exploration geosciences. In: 80th EAGE Annual Conference and Exhibition 2018, Copenhagen, Denmark; 2018. doi: 10.3997/2214-4609.201801619
[38] Pollastro RM, Roberts LNR, Cook TA. Geologic assessment of technically recoverable oil in the Devonian and Mississippian Bakken formation. Assessment of undicsovered oil and gas resources of the Williston Basin Province of North Dakota, Montana and South Dakota. Reston, VA: U.S. Geological Survey; 2013.
[39] Williams JA. Characterization of oil types in Williston Basin. Am Assoc Pet Geol Bull. 1974;58:1243–52. doi: 10.1306/83D91650-16C7-11D7-8645000102C1865D.
[40] Dow WG. Application of oil-correlation and source-rock data to exploration in Williston Basin. Am Assoc Pet Geol Bull. 1974;58:1253–62.
[41] Nesheim TO. Stratigraphic and geochemical investigation of Kukersites (petroleum source beds) within the Ordovician Red River formation, Williston Basin. Am Assoc Pet Geol Bull. 2017;101:1445–71. doi: 10.1306/11111616075.
[42] Pratt BR, Bernstein LM, Kendall AC, Haidl FM. Occurrence of Reefal facies in Red River Strata (upper Ordovician), subsurface Saskatchewan. Summary of investigations 1996. Saskatchewan, Canada: Saskatchewan Geological Survey; 1996. p. 147–52.
[43] Pu R, Kent HQDM, Urban MA. Characterization of Ordovician Midale Field: implication for red river play in Northern Williston Basin, Southeastern Saskatchewan, Canada. Am Assoc Pet Geol Bull. 2003;87:1699–715. doi: 10.1306/07080302021.
[44] Kreis LK, Kent DM. Basement controls on red river sedimentation and hydrocarbon production in Southeastern Saskatchewan. Summary of investigations 2000. Vol. 1. Saskatchewan, Canada: Saskatchewan Geological Survey; 2000. p. 21–42.
[45] Derby JR, Kilpatrick JT. Ordovician red river Dolomite Reservoirs, Killdeer field, North Dakota. Carbonate petroleum reservoirs. New York: Springer; 1985. p. 59–69.
[46] Husinec A. Sequence stratigraphy of the red river formation, Williston Basin, USA: stratigraphic signature of the Ordovician Katian greenhouse to icehouse transition. Mar Pet Geol. 2016;77:487–506. doi: 10.1016/j.marpetgeo.2016.07.003.
[47] Khan DK, Rostron BJ, Margitai Z, Carruthers D. Hydrodynamics and petroleum migration in the upper Ordovician red river formation of the Williston Basin. J Geochem Explor. 2006;89:179–82. doi: 10.1016/j.gexplo.2005.11.072.
[48] Magoon LB, Sánchez RMO. Beyond the petroleum system: geohorizons 1. Am Assoc Pet Geol Bull. 1995;79:1731–6. doi: 10.1306/7834DEE0-1721-11D7-8645000102C1865D.
[49] Magoon LB. The petroleum system – an exploratory tool to find oil and gas and to assist in risk management. In: Howes JVC, Noble RA, editors. Proceedings of the Conference on Petroleum Systems of SE Asia and Australasia, Jakarta, Indonesia. Jakarta, Indonesia: Indonesian Petroleum Association; 1997. p. 25–36.
[50] Magoon LB, Dow WG. The petroleum system – from source to trap. Tulsa, OH: The American Association of Petroleum Geologists; 1991.

[51] Peters KE, Cassa MR. Applied source rock geochemistry. In: Magoon LB, Dow WG, editors. The petroleum system – from source to trap. Tulsa, OH: The American Association of Petroleum Geologists; 1994. p. 93–120.
[52] Pitman JK, Price LC, LeFever JA. Diagenesis and fracture development in the Bakken formation, Williston Basin: implications for reservoir quality in the middle member. Reston, Virginia, USA: US Department of the Interior, US Geological Survey; 2001.
[53] Sonnenberg SA. Toc and pyrolysis data for the Bakken Shales, Williston Basin, North Dakota and Montana. In: Robinson JW, LeFever JA, Gaswirth SB, editors. The Bakken-three forks petroleum system in the Williston Basin. Denver, CO: The Rocky Mountain Association of Geologists; 2011. p. 308–31.
[54] Crovell RA, Balay RH. Geologic model, probabilistic methodology and computer programs for petroleum resource assessment. In: Teleki PG, Mattick RE, Kókai J, editors. Basin analysis in petroleum exploration: a case study from the Bekes Basin, Hungary. Netherlands: Springer Science & Business Media Dordrecht; 1994. p. 295–304.
[55] Dolson J. Understanding oil and gas shows and seals in the search for hydrocarbons. Switzerland: Springer International Publishing; 2016. p. 486.
[56] Ericsson JB, McKean HC, Hooper RJ. Facies and curvature controlled 3d fracture models in a cretaceous carbonate reservoir, Arabian Gulf. Geol Soc Lond Spec Publ. 1998;147:299–312. doi: 10.1144/GSL.SP.1998.147.01.20.
[57] Gudmestad OT, Zolotukhin AB, Jarlsby ET. Petroleum resources with emphasis on offshore fields. UK: WIT Press; 2010. p. 288.
[58] Riley SJ, DeGloria SD, Elliot R. A terrain ruggedness index that quantifies topographic heterogeneity. Intermed J Sci. 1999;5:23–7.
[59] Winstral A, Elder K, Davis RE. Spatial snow modeling of wind-redistributed snow using terrain-based parameters. J Hydrometeorol. 2002;3:524–38. doi: 10.1175/1525-7541(2002)003<0524:SSMOWR>2.0.CO;2.
[60] TGI II Williston Basin Project Working Group. TGI II Williston Basin Database. Manitoba Science, Technology, Energy and Mines. Winnipeg, Manitoba, Canada: Manitoba Geological Survey; 2008.
[61] Roy B. Classement et choix en présence de points de vue multiples (la méthode electre). Revue franjaise d'informatique et de recherche opérationnelle. 1968;2:57–75. doi: 10.1051/ro/196802V100571.
[62] Rogers MG, Bruen M, Maystre L-Y. Electre and decision support: Methods and applications in engineering and infrastructure investment. USA: Springer US; 2000. p. 208. doi: 10.1007/978-1-4757-5057-7.
[63] Adolphe L, Rousval B. Towards an integrated decision process of sustainable urban projects. In: Bragança L, editor. Portugal sb07. Sustainable construction, materials and practices-challenge of the industry for the new millennium. Amsterdam, Netherlands: IOS Press; 2007. p. 418–25.
[64] Zadeh LA. Fuzzy sets. Inf Control. 1965;8:338–53. doi: 10.1016/S0019-9958(65)90241-X.
[65] Chen HC, Fang JH. A new method for prospect appraisal. Am Assoc Pet Geol Bull. 1993;77:9–18. doi: 10.1306/BDFF8B3C-1718-11D7-8645000102C1865D.
[66] Sevkli M. An application of the fuzzy electre method for supplier selection. Int J Prod Res. 2010;48:3393–405. doi: 10.1080/00207540902814355.
[67] Aouam T, Chang SI, Lee ES. Fuzzy madm: an outranking method. Eur J Oper Res. 2003;145:317–28. doi: 10.1016/S0377-2217(02)00537-4.
[68] Abu-Mouti FS, El-Hawary ME. Overview of artificial bee colony (ABC) algorithm and its applications. 2012 IEEE International Systems Conference SysCon 2012. Vancouver, BC: IEEE; 2012. doi: 10.1109/SysCon.2012.6189539.
[69] Karaboga D, Basturk B. A powerful and efficient algorithm for numerical function optimization: artificial bee colony (ABC) algorithm. J Global Optim. 2007;39:459–71. doi: 10.1007/s10898-007-9149-x.
[70] Karaboga D, Basturk B. On the performance of artificial bee colony (ABC) algorithm. Appl Soft Comput. 2008;8:687–97. doi: 10.1016/j.asoc.2007.05.007.
[71] Gozde H, Taplamacioglu MC. Comparative performance analysis of artificial bee colony algorithm for automatic voltage regulator (AVR) system. J Franklin Inst. 2011;348:1927–46. doi: 10.1016/j.jfranklin.2011.05.012.
[72] Akay B, Karaboga D. Artificial bee colony algorithm for large-scale problems and engineering design optimization. J Intell Manuf. 2012;23:1001–14. doi: 10.1007/s10845-010-0393-4.
[73] Karaboga D. An idea based on honey bee swarm for numerical optimization; Report-TR06; Technical report-tr06. Erciyes University, Engineering Faculty, Computer Engineering Department; 2005.
[74] Duan CXH. Artificial bee colony (ABC) optimized edge potential function (EPF) approach to target recognition for low-altitude aircraft. Pattern Recognit Lett. 2010;31:1759–72. doi: 10.1016/j.patrec.2009.11.018.
[75] Duan H, Deng Y, Wang X, Xu C. Small and dim target detection via lateral inhibition filtering and artificial bee colony based selective visual attention. PLoS One. 2013;8:1–12. doi: 10.1371/journal.pone.0072035.
[76] Chou S-Y, Chang Y-H, Shen C-Y. A fuzzy simple additive weighting system under group decision-making for facility location selection with objective/subjective attributes. Eur J Oper Res. 2008;189:132–45. doi: 10.1016/j.ejor.2007.05.006.
[77] Chung C-J, Fabbri AG. Predicting landslides for risk analysis – spatial models tested by a cross-validation technique. Geomorphology. 2008;94:438–52. doi: 10.1016/j.geomorph.2006.12.036.
[78] Hosmer Jr DW, Lemeshow S, Sturdivant RX. Applied logistic regression, 3rd edn. Hoboken, New Jersey: John Wiley & Sons, Inc.; 2013. p. 528. doi: 10.1002/9781118548387.
[79] Gokceoglu HRPC. Spatial modeling in GIS and R for earth and environmental sciences. Cambridge, Massachusetts, USA: Elsevier Inc.; 2019. p. 798. doi: 10.1016/C2017-0-02950-6.
[80] laird WM, Folsom CB. North Dakota's nesson anticline; Report of Investigation 22. Grand Forks, North Dakota: North Dakota Geological Survey; 1956.
[81] Iampen HT, Rostron BJ. Hydrogeochemistry of pre-Mississippian Brines, Williston Basin, Canada – USA. J Geochem Explor. 2000;69–70:29–35. doi: 10.1016/S0375-6742(00)00007-8.
[82] El Taki H, Pratt BR. Synsedimentary deformation in laminated dolostones and evaporates of the Herald formation (red river): signature of late Ordovician tectonic activity in Southern Saskatchewan. Summary of investigations 2009. Vol. 1. Saskatchewan, Canada: Saskatchewan Geological Survey; 2009. p. 1–10.